

CHARACTERISTICS AND FREQUENCY OF LARGE SUBMARINE LANDSLIDES AT THE WESTERN TIP OF THE GULF OF CORINTH

Arnaud Beckers^{1,2*}, Aurelia Hubert-Ferrari¹, Christian Beck², George Papatheodorou³, Marc de Batist⁴, Dimitris Sakellariou⁵, Efthymios Tripsanas⁶, Alain Demoulin¹

¹ Department of Geography, University of Liège, allée du 6 août 2, 4000 Liège, Belgium. Email : beckersarnaud@gmail.com.

² ISTERre, CNRS UMR 5275, University of Savoie, F-73376 Le Bourget du Lac, France.

³ Department of Geology, University of Patras, Greece

⁴ Department of Geology and Soil Science, Gent

⁵ Institute of Oceanography, Hellenic Center for Marine Research, GR-19013 Anavyssos, Greece

⁶ Gnosis Geosciences, Edinburgh, EH10 5JN, U.K.

* Now at: CSD Engineers, Namur Office Park 2, Avenue des dessus de Lives, 5101 Namur, Belgium

Correspondence to: Aurelia Hubert-Ferrari (aurelia.ferrari@ulg.ac.be)

Abstract

Coastal and submarine landslides are frequent at the western tip of the Gulf of Corinth, where small to medium failure events (10^6 - 10^7 m³) occur on average every 30-50 years. These landslides trigger tsunamis, and consequently represent a significant hazard. We use here a dense grid of high-resolution seismic profiles to realize an inventory of the large mass transport deposits (MTDs) that result from these submarine landslides. Six large mass wasting events are identified, and their associated deposits locally represent 30% of the sedimentation since 130ka in the main western Basin. In the case of a large MTD of ~ 1 km³ volume, the simultaneous occurrence of different slope failures is inferred and suggests an earthquake triggering. However, the overall temporal distribution of MTDs would result from the time-dependent evolution of pre-conditioning factors, rather than from the recurrence of external triggers. Two likely main pre-conditioning factors are (1) the reloading time of slopes, which varied with the sedimentation rate, and (2) dramatic changes in water depth and water circulation that occurred 10-12ka ago during the last post-glacial transgression. Such sliding events likely generated large tsunami waves in the whole Gulf of Corinth, possibly larger than those reported in historical sources considering the observed volume of the MTDs.

1 Introduction

The study of marine geohazards through their imprint in the late Quaternary sedimentary record is of great significance, since it can provide further information on geohazard events recorded in historical records, or even extend this record to much earlier times. The identification and recurrence patterns of mass transport deposits (MTDs) resulting from submarine landslides in sedimentary basins and lakes provide valuable information on possibly associated tsunamis as well as their potential trigger (e.g. earthquake). Tsunami hazard is particularly an issue of concern in the Mediterranean Sea where more than 300 tsunamis have been listed in the historical and sedimentary records (Soloviev, 1990; Salamon et al., 2007; Lorito et al., 2008).

This paper focuses on the Gulf of Corinth, Greece, located in the most seismically active part of the Corinth Rift. This area shows one of the largest seismic hazard in Europe (Woessner et al., 2013) and is affected by a tsunami once every 19 years on average, leading to a significant risk (Papadopoulos, 2003; Papatheodorou and Dominey-Howes, 2003). The gulf's western tip is the most active part of the Corinth rift, characterized by an extension of 15 mm.yr^{-1} (Briole et al., 2000), and by frequent submarine or coastal landslides (e.g. Henzen et al., 1966; Papatheodorou and Ferentinos, 1997; Lykousis et al., 2009). Small to medium failure events (10^6 - 10^7 m³) occur on average every 30-50 years (Lykousis et al., 2007a). These landslides trigger tsunamis (Galanopoulos et al., 1964; Stefatos et al., 2006; Tinti et al., 2007) and induce coastal erosion by upslope retrogression (Papatheodorou and Ferentinos, 1997; Hasiotis et al., 2006). Tsunamis reaching an intensity ≥ 4 consequently represent a significant hazard in the western Gulf of Corinth (Beckers et al. 2017), and are documented for the last two millennia from historical

56 sources and onland geological studies (De Martini et al., 2007; Kontopoulos and Avamidis, 2003;
57 Kortekaas et al., 2011). However, these data sets are incomplete.

58
59 A dense grid of high-resolution seismic profiles acquired in this area (Beckers et al., 2015) was used to
60 realize an inventory of the large mass transport deposits (MTDs) that may be interpreted as the result of
61 submarine landslides. Dated from the Late Pleistocene and the Holocene, the mapped mass transport
62 deposits range from 10^6 - 10^9 m³. Average recurrence intervals are presented and discussed, as well as
63 pre-conditioning factors that might have played a role in the occurrence of these large submarine
64 landslides. The MTDs' temporal distribution is discussed, as well as the implications of their occurrence
65 on tsunami hazard.

66 67 2 Setting

68 The western Gulf of Corinth is characterized by a relatively flat deep basin dipping gently to the east.
69 Featuring a narrow canyon in the west, it widens in the east (Delphic Plateau, Fig. 1). It is bordered by
70 steep slopes on all sides (Fig. 1) To the north, it is limited by the Trizonia scarp with slopes ranging
71 from 25° to locally more than 35° and the associated Trizonia Fault (Nomikou et al., 2011); these slopes
72 are mostly devoid of sediments which are trapped in the bay areas to the north (Fig. 1B). To the south,
73 the western Gulf is bordered by 400m high Gilbert deltas built by the Erineos, Meganitis and Selinous
74 ivers that lie in front of the active Psathopyrgos, Kamari and Aigion Faults running along or near the
75 coastline. Delta fronts have 15° to 35° slopes incised by gullies (Lykousis et al., 2007; Nomikou et al.
76 2011) and consist of a thick pile of fine grained sediments. The delta-front sediments accumulated over
77 the Holocene and the previous glacial-interglacial period have thicknesses, respectively, larger than 50m
78 and 100 m (Fig. 1B and 1C; Beckers, 2015; Beckers et al., 2016). At the north-western end of the Gulf,
79 lies the largest fan-delta of the Mornos River that drains 913 km² and is by far the largest watershed
80 among the rivers flowing toward the westernmost Gulf of Corinth (Fig. 1A). The delta fronts are highly
81 unstable (Ferentinos et al., 1988; Lykousis et al., 2009), which favours frequent submarine landsliding
82 (Stefatos et al., 2006; Tinti et al., 2007; Fig. 1B). During the last centuries, submarine landslides have
83 been triggered by earthquakes and by sediment overloading on steep slopes (Galanopoulos et al., 1964;
84 Heezen et al., 1966). Numerous debris-flow deposits and mass-transport deposits (MTDs) have thus
85 accumulated at the foot of the deltas (Ferentinos et al., 1988; Beckers et al., 2016; Fig. 1B). Alongside
86 these gravity-driven sedimentary processes, contour-parallel bottom-currents also influenced sediment
87 transport in this area (Beckers et al., 2016).

88 89 3 Data and Method

90 Two seismic reflection surveys were carried out in 2011 and 2014 with the aim of imaging the
91 subsurface below the westernmost Gulf of Corinth floor. The data were acquired by the Renard Center
92 of Marine Geology of the University of Ghent along a grid of 600 km high-resolution seismic profiles
93 with a "CENTIPEDE" Sparker seismic source combined with a single-channel high-resolution streamer
94 as receiver (see details in Beckers et al., 2015). The expected vertical resolution at depth is ~1 m. In the
95 deep basin (Canyon and Delphic Plateau areas, Fig. 1), the maximum penetration depth below the sea
96 floor is about 360 ms TWTT (two-way travel time) to the east and about 100 ms TWTT to the west, i.e.,
97 270-360 m and 75-100 m, respectively.

98 The inferred stratigraphic framework (Beckers et al., 2015) permits to identify two temporal horizons.
99 Reflector 1 has been mapped in the whole study area, except in a basin west of the Trizonia Island (Fig.
100 2). This reflector corresponds to the beginning of the last post-glacial transgression, at 10.5-12.5 ka
101 (Cotterill, 2006; Beckers et al., 2016). The second temporal horizon, 'reflector 2', has been mapped in
102 the Delphic Plateau area only. It corresponds to the marine isotopic stage 6 to 5 transgression, which
103 occurred at ca. 130 ka.

104
105 **Figure 1.** Study area with at the top, the fault map of Beckers et al. (2015) with the bathymetry from
106 Nomikou et al. (2011), in the middle, the morphosedimentary map of Holocene deposits of Beckers et
107 al. (2016), at the bottom the isopach maps of the Holocene (Right ; Beckers et al., 2016), and of the
108 preceding period from 10 to 130 ka (Left ; Beckers, 2015). White areas in the bottom figures correspond

Aurélia Ferrari 7/2/2018 15:01
Deleted: It

Aurélia Ferrari 7/2/2018 15:01
Deleted: to the south

Aurélia Ferrari 7/2/2018 15:02
Deleted: and, a

Aurélia Ferrari 7/2/2018 15:02
Deleted: its

Aurélia Ferrari 7/2/2018 15:03
Deleted: by

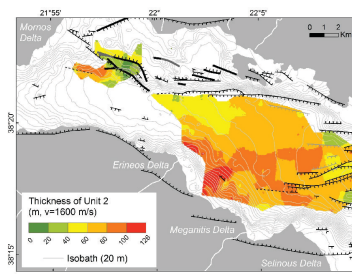
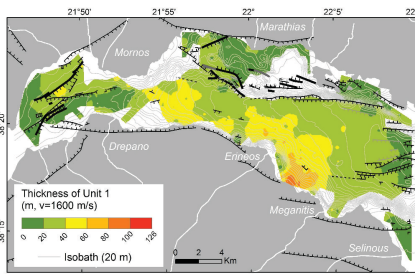
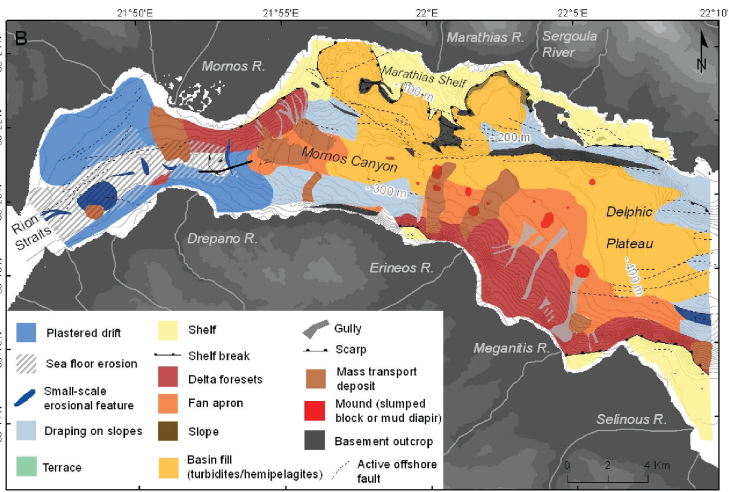
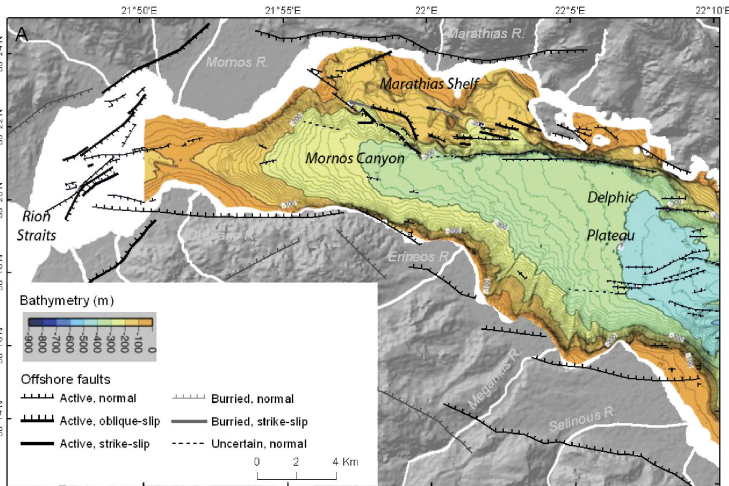
Aurélia Ferrari 7/2/2018 15:04
Deleted: but some also occurred because of

Aurélia Ferrari 7/2/2018 15:04
Deleted: see also a facies map in

Aurélia Ferrari 13/2/2018 10:52
Deleted: l

117
118

to the ones with poor data or with an absence of stratigraphic marker. Grey curves in middle and bottom figures are sea floor contour lines interpolated from the seismic grid.



119
120
121

Unknown
Formatted: Font:Times New Roman, Bold

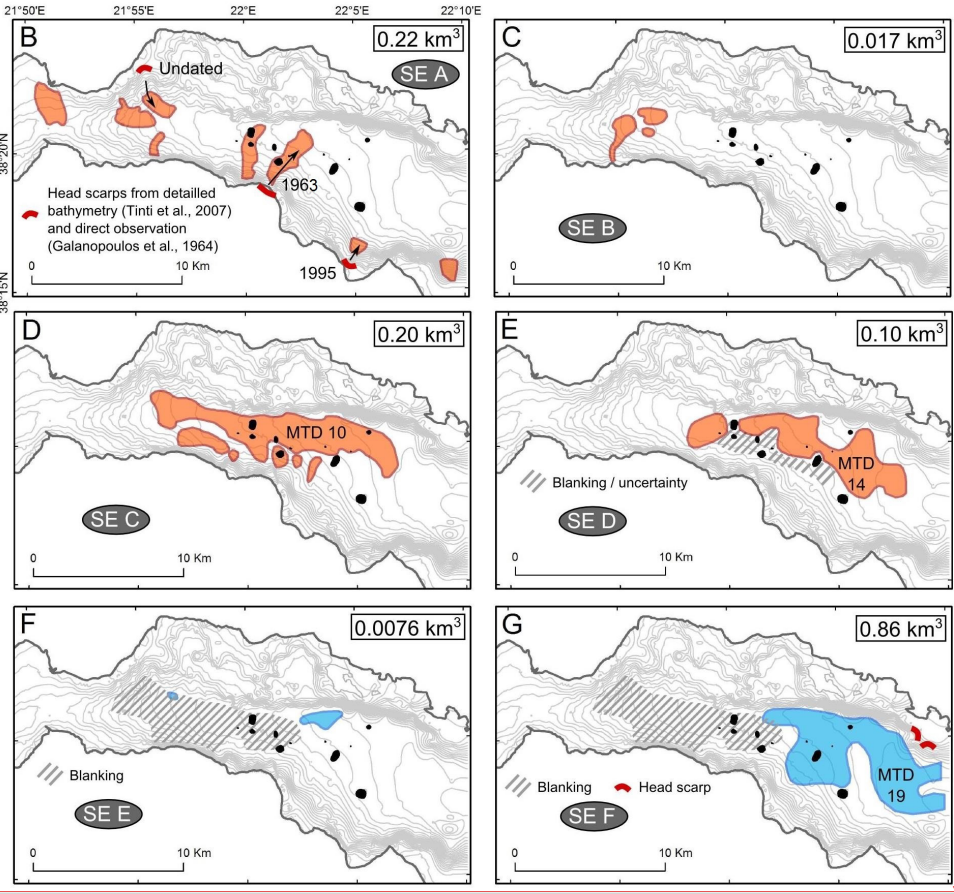
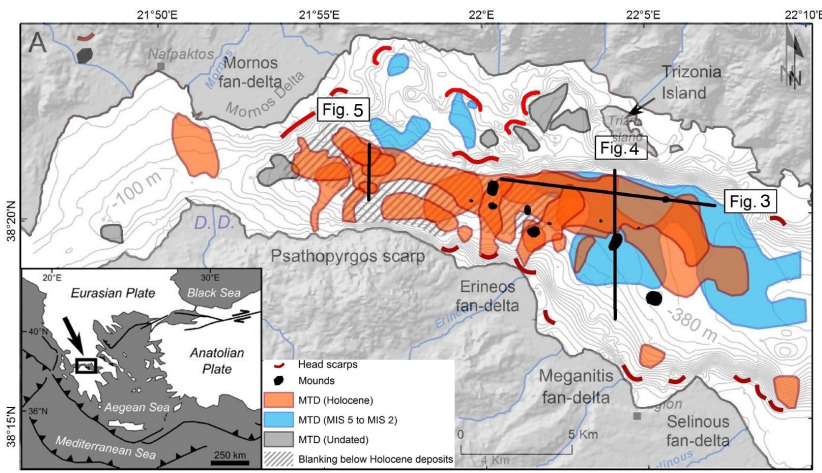
122
123 **Figure 2.** Inventory of mass transport deposits (MTDs) at the westernmost Gulf of Corinth for the last ca.
124 130 ka. A) spatial extent and age of the 32 MTDs with in grey seismic grid used for the inventory; B) to G):
125 spatial distribution of MTDs for each sliding event (SE). Grey lines show the seismic grid. Black dots
126 represents the mounds described in Beckers et al. (2016a). The total volume of sediments in the MTDs is
127 mentioned for each sliding event.

Aurélia Ferrari 13/2/2018 10:03

Deleted: 1

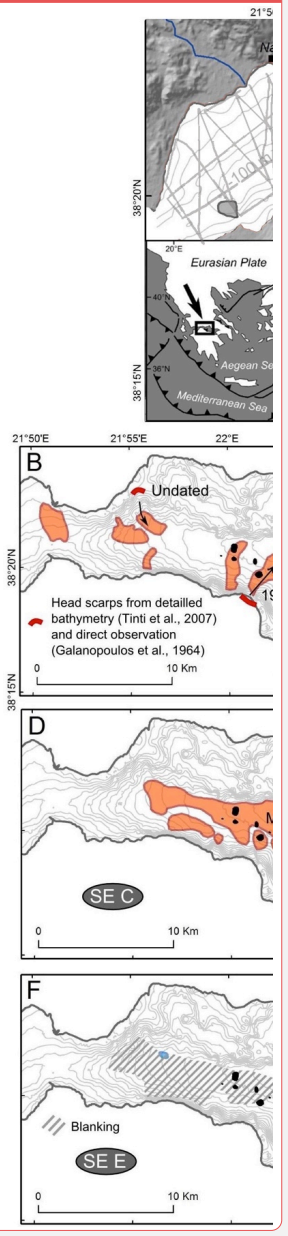
Aurélia Ferrari 13/2/2018 10:56

Deleted: .



Unknown
Formatted: Font:Times New Roman

Aurélia Ferrari 13/2/2018 11:16



Deleted:

130
131

133
134 Mass transport deposits have been identified on high-resolution seismic profiles based on their typical
135 seismic facies made of discontinuous to chaotic reflections. The shape of each deposit in map view has
136 been interpolated manually, based on the seismic profiles that intersect the MTD. Thicknesses were
137 derived using a seismic velocity of 1600 m s^{-1} (Bell et al., 2009). For the largest MTDs, an inverse
138 distance weighted interpolation between thickness data points was used to derive isopach maps of the
139 deposits and estimate their total volume. However, this interpolation method cannot be used for smaller
140 MTDs crossed only by a few seismic lines. In this case, the volume was estimated by multiplying the
141 MTD surface by an average thickness value. The derived volumes of small MTDs (surface area $< \sim 2$
142 km^2) are thus rough estimates, especially for MTDs crossed by only two or three seismic profiles. By
143 contrast, volume estimates of large MTDs (surface area $> \sim 5 \text{ km}^2$) are more accurate with volume
144 uncertainties probably $< 20 \%$.
145

146 | Landslide headscarps have been mapped using three different data sources, namely (1) the grid of high-
147 resolution seismic profiles acquired for this study, (2) an analysis of three submarine landslides in the
148 study area by (Tinti et al., 2007), and (3) a 3D bathymetric view of the area between the Erineos and the
149 Selinous fan-deltas from Lykousis et al. (2009). In the absence of multi-beam bathymetry over the
150 whole study area, the mapping of Late Quaternary submarine landslides head scarps presented here is
151 certainly not exhaustive. The location of potential headscarps associated with the largest MTDs mapped
152 in the following are also discussed considering the location of the thickest deposits and the nearest
153 upslope delta-front sediments.
154

155 4 Results

156 Thirty-two MTDs have been imaged in the study area, from which 67% are located in the large E-W
157 trending basin located below the flat deep basin (Canyon and Delphic Plateau, Fig. 2). Eight MTDs have
158 been identified in the northern margin of the Gulf, and two in the Nafpaktos Bay to the west of the
159 Corinth Gulf (Fig. 2). The age of 24 MTDs has been estimated based on the stratigraphic framework
160 developed previously (Beckers et al., 2015): 19 of them occurred during the Holocene and 5 during the
161 period between $\sim 130 \text{ ka}$ and $\sim 11.5 \text{ ka}$. A finer stratigraphy could be established in the flat deep basin,
162 thanks to the relative continuity of the reflectors over this 20 km-wide area. Consequently, this work
163 focuses on the 22 MTDs located in this area.
164

165 In the Delphic Plateau basin (eastern part of the deep flat basin), most MTDs are imaged as lenticular
166 bodies of low-amplitude, incoherent reflections (Fig. 3 and 4). They generally have a flat upper surface
167 and pinch out on their margins. Their thickness ranges between a few meters, which is the minimal
168 thickness for a MTD to be imaged with the seismic system used, and 53 meters. The geometry and
169 seismic facies indicate subaquatic mass-flow deposits (e.g. Moernaut et al., 2011, Strasser et al., 2013).
170 The seismic facies of many MTDs also suggests a fine-grained lithology. However, this statement must
171 be viewed cautiously considering the uncertainties on the interpretation of seismic facies in terms of
172 grain-size, especially for reworked sediments. For instance, failure of coarse-grained deltaic deposits
173 commonly result to their total disaggregation and transformation into grain flows and turbidity currents,
174 whereas finer grained deposits evolve as landslides and cohesive debris flows (Tripsanas et al., 2008).
175

176 In the Canyon basin (western part of the deep flat basin), the MTDs present the same general
177 characteristics but the reflector pattern is more variable (Fig. 5). Some high-amplitude reflections and
178 coherent layering are observed in some MTDs, suggesting coarser-grained sediments and locally
179 preserved stratigraphy.
180

181 Finally, some of the 22 MTDs show sediment/fluid escape features at their top (Fig. 3 and 5). Such
182 features might have been produced by the combination of under-compaction (excess pore water
183 pressure) and shaking, thus possibly pointing to paleoearthquakes (e.g. Moernaut et al., 2007, Moernaut
184 et al., 2009). The volume of sediments in individual MTDs ranges from $7.7 \cdot 10^5$ to $8.6 \cdot 10^8 \text{ m}^3$ (Fig. 6).
185

186 | Landslide headscarps have been identified in different parts of the study area (Fig. 2A). They are
187 particularly numerous on the slopes of the large Gilbert fan-deltas of the Erineos, Meganitis and

Aurélia Ferrari 21/2/2018 14:15

Deleted: Some potential l

Aurélia Ferrari 13/2/2018 10:52

Deleted: 1

Aurélia Ferrari 13/2/2018 10:52

Deleted: 1

Aurélia Ferrari 13/2/2018 10:52

Deleted: 2

Aurélia Ferrari 13/2/2018 10:53

Deleted: 3

Aurélia Ferrari 7/2/2018 15:17

Deleted: , which would make them different from the coarse-grained deltaic deposits that are known to fail relatively frequently along the southern coast

Aurélia Ferrari 13/2/2018 10:53

Deleted: 4

Aurélia Ferrari 7/2/2018 15:18

Deleted: revealing

Aurélia Ferrari 7/2/2018 15:18

Deleted: layering

Aurélia Ferrari 13/2/2018 10:53

Deleted: 2

Aurélia Ferrari 13/2/2018 10:53

Deleted: 4

Aurélia Ferrari 13/2/2018 10:56

Deleted: 5

Aurélia Ferrari 13/2/2018 10:53

Deleted: 1

204 Selinous at the south-east and Mornos at the north-west. In the latter area, one up to 50 m-high
205 headscarp is imaged in the seismic data. The absence of undisturbed sediments on the erosional slope,
206 downslope of the headscarp, suggests a recent age. In the Erineos, Meganitis and Selinous fan-delta
207 slopes, headscarps have been identified in the seismic data and on the 3D view from Lykousis et al.
208 (2009). Most of these headscarps are relatively small, lunate-shaped features linked to gullies. Two large
209 head scarps are localized on the northern slope as well (Fig. 2A). Linking a headscarp to a particular
210 MTD is often delicate for two reasons. First, the age of the headscarps is difficult to estimate because
211 these erosional forms often affect steep slopes in coarse-grained deposits, making impossible to define a
212 seismic stratigraphy in such areas. Second, at the foot of these erosional slopes, a high number of MTDs
213 are stacked (e.g., Fig. 3). Exceptions, detailed hereafter, concern three recent submarine landslides and
214 the largest observed MTD (MTD 19 in SE F).
215

Aurélia Ferrari 13/2/2018 10:53

Deleted: 1

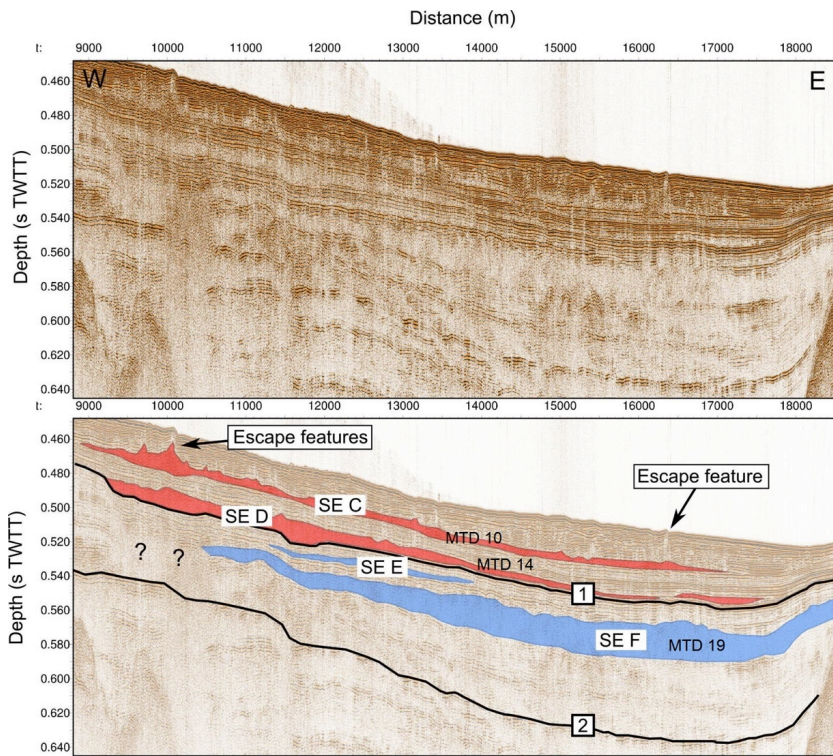
Aurélia Ferrari 13/2/2018 10:53

Deleted: 2

218
219
220
221
222
223
224

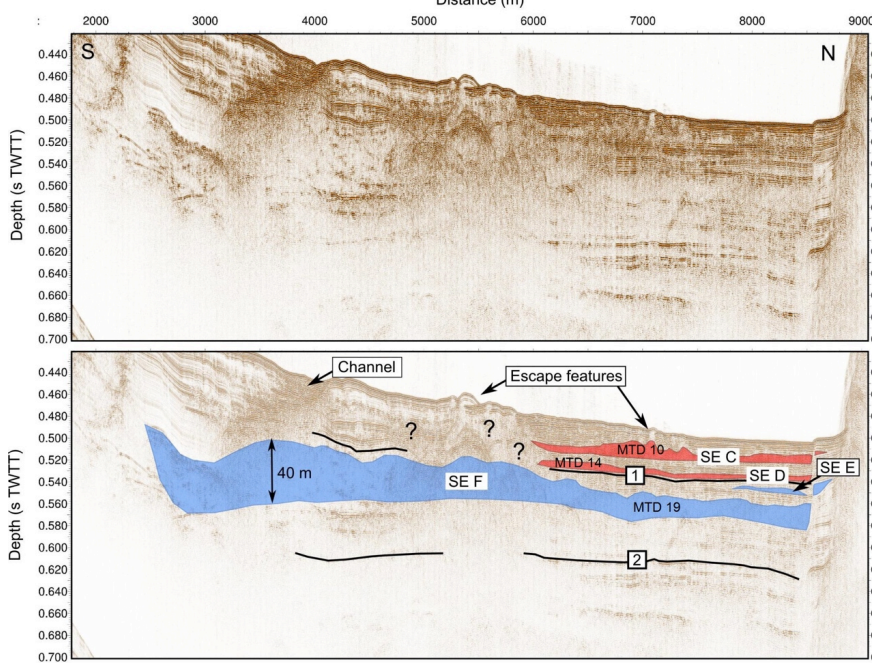
Figure 3. E-W Sparker seismic profile showing the mass transport deposits imaged in the Delphic Plateau basin. See the location of the profile in Fig. 2, Horizon [1] indicates the beginning of the last post-glacial transgression, at 10.5-12.5 ka and horizon [2] the marine isotopic stage 6 to 5 transgression, which occurred at ca. 130 ka (Cotterill, 2006; Beckers et al., 2015; 2016)

Aurélia Ferrari 13/2/2018 10:30
Deleted: 2
Aurélia Ferrari 13/2/2018 10:53
Deleted: 1



225
226

229 | **Figure 4.** S-N Sparker seismic profile showing the mass transport deposits imaged in the Delphic Plateau
 230 basin. Questions marks highlight units of remobilized sediments that are difficult to localize in the
 231 stratigraphic framework. See the location of the profile in Fig. 2.



232
 233

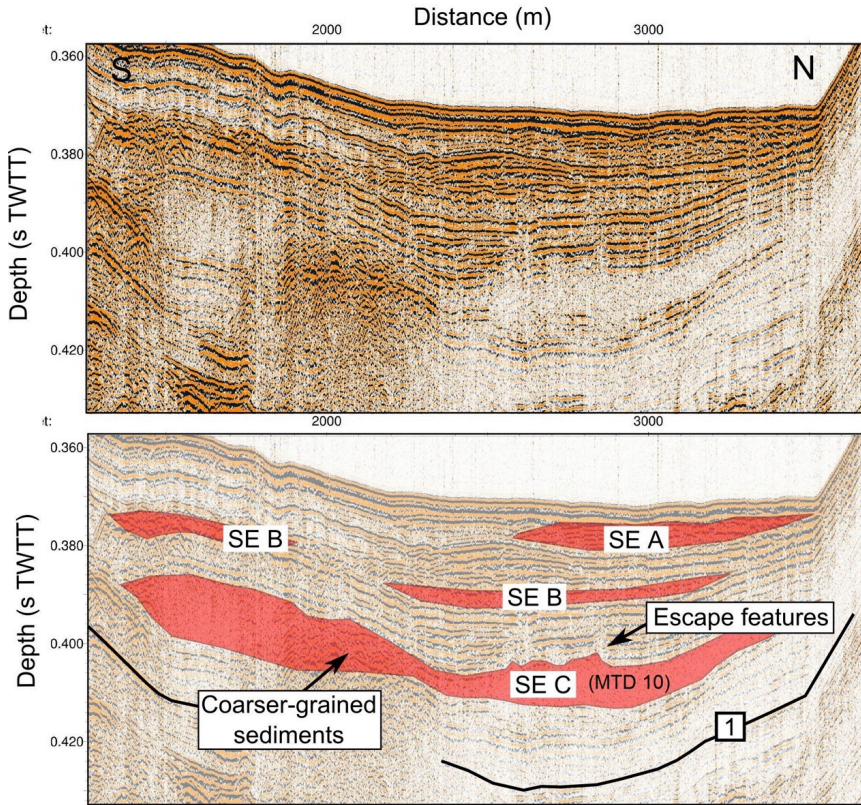
Aurélia Ferrari 13/2/2018 10:30

Deleted: 3

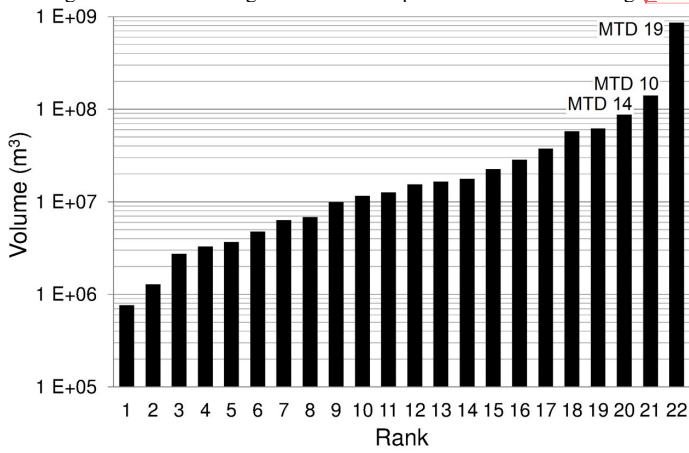
Aurélia Ferrari 13/2/2018 10:53

Deleted: 1

236 | **Figure 5** Examples of mass transport deposits in the Canyon basin. See the location of the Sparker seismic
 237 | profile in Fig. 2



238
 239
 240 | **Figure 6** Volume distribution of the 22 MTDs studied in the Canyon and the Delphic Plateau basins. The
 241 | names given to the three largest MTDs correspond to the notation in Fig. 2.



242
 243
 244

Aurélia Ferrari 13/2/2018 10:30
 Deleted: 4
 Aurélia Ferrari 13/2/2018 10:54
 Deleted: 1

Aurélia Ferrari 13/2/2018 10:30
 Deleted: 5
 Aurélia Ferrari 13/2/2018 10:54
 Deleted: 1

249 The stratigraphic position of MTDs in the Canyon and in the Delphic Plateau basins is not random. Most
250 of them are clustered and are defining multi-MTDs temporal "events", based on common un-deformed
251 underlying or overlying reflections that can be followed across the basin. Such correlations suggest that
252 six events of large clustered submarine mass wasting occurred over the last 130 ka. Two sliding events
253 (SE) are represented by clustered MTDs located between reflectors 2 and 1 (SE E and F). The four
254 others occurred during the Holocene: SE D comprises MTDs deposited just on top of the reflector 1, SE
255 C is located in the middle of the Holocene sequence, SE B somewhat higher, and finally SE A includes
256 MTDs at or near the sea floor responsible for its present-day hummocky topography. The spatial
257 distribution and the total volume of the MTDs associated to each of these events are represented in Fig.
258 2.

Aurélia Ferrari 7/2/2018 15:24

Deleted: may be assigned to

259
260 In some zones (Fig. 2), the existence or the geometry of MTDs is difficult to evaluate because of seismic
261 blanking and strong chaotic reflections affecting some stratigraphic intervals. Above reflector 1, the
262 stratigraphy is clear except regarding the southern extension of MTD 14 in SE D. The low amplitude,
263 almost transparent reflections characterizing the MTD deposit extends until a more chaotic and thicker
264 deposit associated with surface mounds (Fig. 5). We could not decipher if the chaotic reflections that
265 disturb the seismic stratigraphy was associated with MTD 14 in SE D or in relation with sediment
266 remobilization from the underlying sliding event F (Fig. 4). So the mapped extension of MTD 14 in Fig.
267 2E is conservative and considered as a minimum. Below reflector 1, the amplitude of the reflectivity
268 sharply decreases, which is a characteristic of lowstand deposits in the Gulf (Bell et al., 2008), and
269 blanking occurs in two areas. In the Canyon area, a wide blanking area exists at a depth of about 50 to
270 70 m below the sea floor, a few meters below reflector 1, in direct continuity with the delta of the
271 Mornos River. Blanking is thus a low-stand related feature and might correspond to coarse grained,
272 organic rich sediments of the Mornos River. Consequently, the stratigraphy of MTDs between reflectors
273 2 and 1 is well established only below the Delphic Plateau. The other area associating with blanking and
274 strongly disturbed sediments forming mounds occurs at the junction between the Canyon and the
275 Delphic plateau at the foot of the Erineos foreset beds, at a depth similar to SE F. Its origin is unknown,
276 but it might be related to an MTD deposit in relation with MTD 19.

Aurélia Ferrari 7/2/2018 15:30

Deleted: that outcrop

Aurélia Ferrari 13/2/2018 10:54

Deleted: I

Aurélia Ferrari 13/2/2018 10:55

Deleted: I

Aurélia Ferrari 6/2/2018 10:59

Deleted:

277
278 The definition of sliding events reflects a clustering of submarine landslides in a relatively short period
279 of time. It does not necessarily imply a synchronous occurrence of all submarine landslides included in
280 one event. Indeed, the accuracy of the correlation between separated MTDs that are interpreted to
281 belong to the same sliding event is in the order of one or two reflections in the seismic data. Deciphering
282 the exact MTD chronology within a sliding event was not possible because of the discontinuous
283 character of many reflections and the relatively large distance that separates some MTDs (up to 8.5 km).
284 This "stratigraphical" uncertainty corresponds to ~1-2 meters of sediment or, based on sedimentation
285 rate estimates, sliding events represent a set of MTDs that occurs over a period of 300 to 1000 years
286 (Lykousis et al., 2007).

Aurélia Ferrari 6/2/2018 11:01

Deleted: This so far poorly understood blanking area might correspond to a large MTD from the sliding events E or F, or to coarse-grained fluvio-deltaic deposits.

Aurélia Ferrari 21/2/2018 14:25

Deleted: However, there, the spatial extent of the MTDs from SE D (Fig. 1E) is uncertain, owing to chaotic reflections that disturb the seismic stratigraphy possibly in relation with sediment remobilization from the underlying sliding event F (Fig. 3).

Aurélia Ferrari 7/2/2018 15:28

Deleted: This uncertainty results from

287
288 Individual sliding events are characterized as follows (Fig. 2B to G):

Aurélia Ferrari 7/2/2018 15:29

Deleted: of sedimentation

Aurélia Ferrari 13/2/2018 10:54

Deleted: I

Aurélia Ferrari 7/2/2018 15:31

Deleted: that outcrop

Aurélia Ferrari 13/2/2018 10:54

Deleted: I

289
290 *Sliding event A:* Eight MTDs at or near the sea floor have been identified. Their spatial distribution
291 indicates that three of them result from slope failures in the Mornos delta and five from failures at
292 different locations along the southern margin (Fig. 2). The volumes of these MTDs range between ~4.7
293 10^6 m³ and ~6.2 10^7 m³, and the total volume of the eight MTDs is about ~2.2 10^8 m³.

294
295 Some of these MTDs correspond to submarine landslides described in the literature (Galanopoulos
296 1964; Papatheodorou and Ferentinos 1997; Tinti et al., 2007). The MTD located north-east of the
297 Erineos delta results from a coastal landslide on this fan-delta in 1963, which triggered a large tsunami
298 on both sides of the Gulf (Galanopoulos et al., 1964; Stefatos et al., 2006). The MTD located at the foot
299 of the Meganitis fan-delta likely corresponds to a coastal landslide triggered by the 1995 Aigion
300 earthquake on this delta (Papatheodorou and Ferentinos 1997; Tinti et al., 2007). The volumes of
301 sediments involved in these two landslides have been estimated at ~4.6 10^7 m³ from the data presented
302 by Stefatos et al. (2006), and about ~2.8 10^7 m³ by Tinti et al. (2007), respectively. The corresponding
303 volumes estimated from the present study are ~6.1 10^7 m³ and ~2.2 10^7 m³, which are in the same order

324 of magnitude. Another well preserved but undated landslide headscarp has been identified by Tinti et al.
325 (2007) on the eastern side of the Mornos fan-delta (Fig. 2). These authors estimated the volume of the
326 sliding mass at $\sim 9 \cdot 10^6 \text{ m}^3$. Our data show a MTD located about 1 km downslope of the scarp, with an
327 estimated volume of $\sim 9.9 \cdot 10^6 \text{ m}^3$ that fits remarkably well with the volume derived from the geometry of
328 the scarp.

329
330 *Sliding event B:* The sliding event B comprises three MTDs located at the western tip of the canyon.
331 They are located between 12 and 16 m below the sea floor and are relatively thin (~ 2 to 5 m thick) (Fig.
332 5). Location and geometry of the MTDs indicate that they result from slope failures in the Mornos fan-
333 delta and in the Psathopyrgos scarp. The total volume of these MTDs is about $\sim 1.7 \cdot 10^7 \text{ m}^3$.

334
335 *Sliding event C:* The sliding event C includes one large MTD extending over a wide area below the
336 Canyon and a part of the Delphic Plateau (MTD 10), and smaller deposits located at the foot of the
337 southern slopes, in the Psathopyrgos scarp and Erineos fan-delta areas. The thickness of MTD 10 is
338 shown in Fig. 7. Five local maxima are connected by a 2-5 m thick sheet of low-amplitude incoherent
339 reflections. The thickest sediment accumulation (30 m) is located at the foot of the Erineos fan-delta.
340 The other maxima are 5 to 10 m thick. Two are located at the western tip of the MTD and suggest
341 sediment inputs from the Mornos fan-delta area and from the Psathopyrgos scarp (Fig. 5). The last two
342 maxima are located in the south-eastern part of the deposit, with a possible source in the Erineos fan-
343 delta. The total volume that failed during sliding event C is about $\sim 2.0 \cdot 10^8 \text{ m}^3$, including $\sim 1.4 \cdot 10^8 \text{ m}^3$ for
344 MTD 10.

345
346 **Figure 7.** Thickness of the largest MTDs deduced from the interpretation of Sparker seismic profiles with
347 probable sediment paths indicated by red arrows (bold arrow: main sources). Contours represent the sea floor
348 bathymetry interpolated from the Sparker data (one line every 20 m). Left: MDT 10 in sliding event C, the
349 largest MDT from the sliding event C. Center: Thickness of MDT 14, the largest of the two MTDs that define
350 the sliding event D. Bottom: The largest MTD from the presented inventory (MTD 10, sliding event F). The
351 black bold lines represent two landslide head scarps likely linked to the MTD. The dotted line shows the
352 location of the seismic profile in Fig. 8.

353

Aurélia Ferrari 13/2/2018 10:58
Deleted: 1

Aurélia Ferrari 13/2/2018 10:58
Deleted: 4

Aurélia Ferrari 13/2/2018 10:58
Deleted: 6

Aurélia Ferrari 13/2/2018 10:58
Deleted: 4

Aurélia Ferrari 13/2/2018 10:30
Deleted: 6

Aurélia Ferrari 21/2/2018 14:28
Formatted: Font:Not Bold

Aurélia Ferrari 21/2/2018 14:28
Deleted: Thickness of

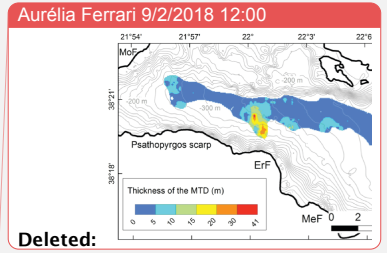
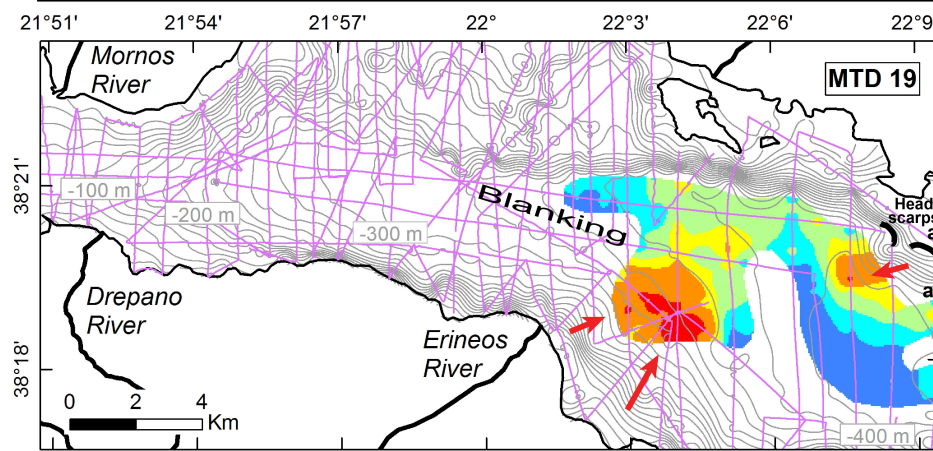
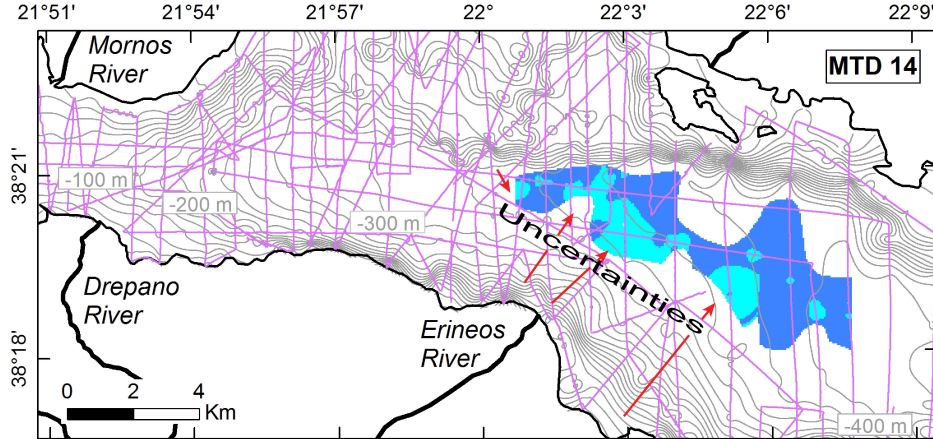
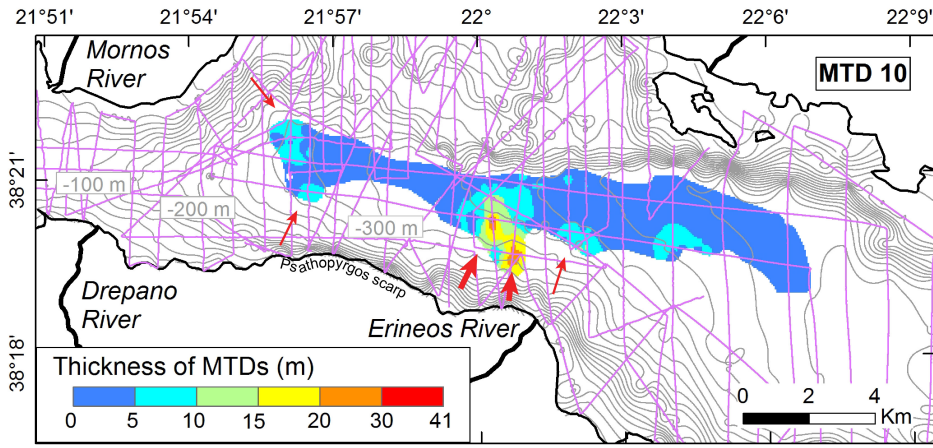
Aurélia Ferrari 21/2/2018 14:29
Deleted: , deduced from the interpretation of Sparker seismic profiles

Aurélia Ferrari 21/2/2018 14:30
Deleted: Contours represent the sea floor bathymetry (one line every 20 m). MoF = Mornos fan-delta, ErF = Erineos fan-delta, MeF = Meganitis fan-delta. -

Aurélia Ferrari 21/2/2018 14:30
Deleted: , deduced from the interpretation of Sparker seismic profiles. Contours represent the sea floor bathymetry (one line every 20 m). ErF = Erineos fan-delta.

Aurélia Ferrari 21/2/2018 14:31
Deleted: - ... [1]

Aurélia Ferrari 13/2/2018 10:58
Deleted: 7. EF = Erineos fan-delta, SF = Selinous fan-delta.



378 The geometry of MTD 10 suggests that slope failures occurred simultaneously in different parts of the
379 westernmost gulf during sliding event C. The main source of sediment was the Erineos fan-delta, as
380 attested by the location of the thickest sediment accumulation in the MTD 10, and by the presence of
381 other MTDs at the same stratigraphic level between MTD 10 and the Erineos fan-delta (Fig. 2D).

382
383 *Sliding event D:* Two MTDs are located just on top of reflector 1 and define the sliding event D. Both
384 are between ~2 and 10 m thick and spread over several square kilometres in front of the Erineos and
385 Meganitis fan-deltas. The southern limit of the deposits is unclear, because the stratigraphy in the area
386 between the two MTDs and the Erineos pro-delta is poorly constrained (hatching on Fig. 2E and
387 question marks in Fig. 4). In this area, it is not sure whether the incoherent reflections located south of
388 the SE D MTD at a similar depth represent the same MTD or the underlying, older (SE F), MTD or
389 escape features from the latter, as suggested by the escape features observed at the sea floor (Fig. 4).

390
391 The isopach map of the largest deposit (MTD 14) is shown in Fig. 7, and suggests that it was fed by
392 slope failure(s) mostly south of the Delphic Plateau probably from the Erineos Delta Fan. The volume of
393 MTD 14 is estimated at $\sim 8.7 \cdot 10^7 \text{ m}^3$, and the total volume of SE D MTDs is about $\sim 1.0 \cdot 10^8 \text{ m}^3$.
394 Considering uncertainties on the geometry of these MTDs' southern edges, these values are minimum
395 estimates.

396
397 *Sliding event E:* Two MTDs define this sliding event. The largest one is located in the Delphic Plateau
398 basin, just south of the Trizonia Island and has a volume of $\sim 6.6 \cdot 10^6 \text{ m}^3$. The second is much smaller
399 ($\sim 1.3 \cdot 10^6 \text{ m}^3$) and is located in the Canyon basin. Stratigraphically, both are located a few meters below
400 reflector 1. However, they are horizontally 8.5 km apart, making the correlation uncertain. The total
401 volume of the two MTDs in sliding event E is $\sim 7.9 \cdot 10^6 \text{ m}^3$.

402
403 *Sliding event F:* The sliding event F is defined by one single large complex MTD (MTD19) (Fig. 2).
404 This deposit is located in the Delphic Plateau basin. Stratigraphically, it belongs to the upper part of the
405 unit between reflectors 2 and 1, suggesting that this event occurred during the last glacial period. With a
406 volume of $\sim 8.6 \cdot 10^8 \text{ m}^3$, this deposit is the largest MTD of the present inventory. It covers an area of 41
407 km^2 , i.e., almost the whole Delphic Plateau. The isopach map reveals a main up to 50 m-thick sediment
408 accumulation in the south-western part of the deposit (Fig. 4) and another ~30 m-thick depocenter in the
409 north-eastern part (Fig. 7). The MTD is imaged as low amplitude, almost transparent chaotic reflections
410 except in the thickest part where high-amplitude reflections indicate coarser-grained sediments and
411 locally preserved layering (Fig. 4). No sedimentological structure has been observed between the two
412 maxima in thickness.

413
414 The geometry of the deposit and the absence of clear structure between the two depocenters support the
415 idea of at least two simultaneous slope failures having generated this large MTD. The largest failure
416 occurred south of the MTD, on the Meganitis or the Erineos fan-delta slopes. Considering the large
417 volume of sediments in the south-western part of the MTD, we expected a major scar across the
418 southern slopes, which we could not retrieve however neither from the seismic data, nor from published
419 bathymetries (Lykousis et al., 2009). Indeed, dozens of small head scarps and gullies dissect the slopes
420 of the offshore Erineos and Meganitis deltas, making difficult the identification of large features. **The**
421 **second depocenter occurs near the north-eastern edge of the Delphic Plateau Basin, and upslope two**
422 **submarine landslide headscarps located 2 km from each other were evidenced in seismic profiles (bold**
423 **lines in Fig. 7). Cut through stratified hemipelagites, they are 11 and 15 m-high and are located at 300**
424 **and 195 m below the sea level, respectively (Fig. 8). Although it is not possible to reconstruct the 3D**
425 **geometry of a single large headscarp from the seismic data, this would be a good candidate source of the**
426 **thick sediment accumulation in the north-eastern part of MTD 19.**

427
428 **Figure 8.** Sparker seismic profile illustrating a submarine landslide head scarp that is probably linked to the
429 MTD 19. See the location of the profile in Fig. 7.

430

Aurélia Ferrari 13/2/2018 10:58

Deleted: 1

Aurélia Ferrari 13/2/2018 10:58

Deleted: 1

Aurélia Ferrari 13/2/2018 10:58

Deleted: 3

Aurélia Ferrari 13/2/2018 10:59

Deleted: 3

Aurélia Ferrari 13/2/2018 10:59

Deleted: 6

Aurélia Ferrari 13/2/2018 10:59

Deleted: 1

Aurélia Ferrari 13/2/2018 10:59

Deleted: 3

Aurélia Ferrari 13/2/2018 10:59

Deleted: 6

Aurélia Ferrari 13/2/2018 10:59

Deleted: 3

Aurélia Ferrari 21/2/2018 14:46

Deleted: T

Aurélia Ferrari 21/2/2018 14:46

Deleted: are highlighted

Aurélia Ferrari 21/2/2018 14:46

Deleted: by

Aurélia Ferrari 21/2/2018 14:46

Deleted: on the slope north of the MTD

Aurélia Ferrari 13/2/2018 10:59

Deleted: 6

Aurélia Ferrari 13/2/2018 11:00

Deleted: 7

Aurélia Ferrari 21/2/2018 14:47

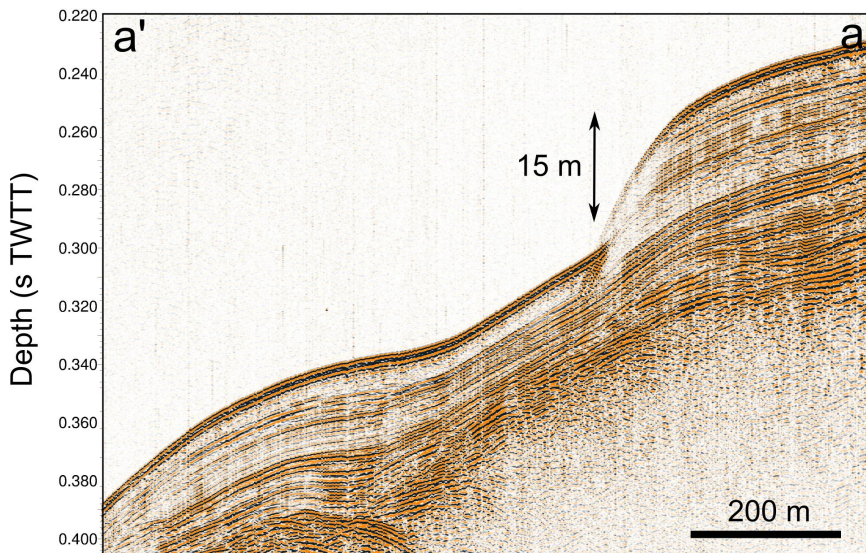
Deleted: might

Aurélia Ferrari 13/2/2018 10:31

Deleted: 7

Aurélia Ferrari 13/2/2018 11:00

Deleted: 6



449
450

5 Discussion

5.1 Limitations of the analysis

453

456 Before discussing the implications of the presented MTD inventory in the deep flat basin in terms of
457 sediment sources and triggering mechanisms, it is necessary to point out that only submarine landslides
458 that have remobilized a sufficient quantity of sediments down to the basin floor are considered here.
459 Moreover, the high-resolution seismic profiling system used does not permit identifying MTDs thinner
460 than ~1 m. Consequently, our inventory is incomplete and could be refined by the use of very-high
461 resolution seismic profiling systems and long cores.

462

5.2 Sediment sources

463

465 According to the mapping of the thickness of the deposits, large sliding events in the westernmost Gulf
466 of Corinth mainly result from slope failures in, or close to, the Gilbert-type fan-deltas. Large sediment
467 volumes were trapped in these deltas during the Holocene. As shown in Figure 1, Holocene foreset beds
468 reach 40 to 60 m in thickness on average in the Eroneos and Meganitis fan-deltas, and sediment
469 accumulation during the Holocene exceeding 100 m have been observed locally in between. These are
470 the sources of MTD 10 in sliding event C and MTD 14 in sliding event D. The remarkable amount of
471 sediments delivered to the gulf of Corinth during the Holocene probably results from large volumes of
472 sediments stored onland during the last glacial period that were mobilized from river floodplains and
473 colluvial deposits to rivers deltas. Widespread soil erosion resulting from human deforestation and
474 agriculture during the second half of the Holocene also contributed to increase sediment fluxes in this
475 period. Similarly, the previous period considered here spanning ~130 ka to ~11 ka is also characterized
476 by a large sediment accumulation with a pile of 60 to 100 m forming the delta fronts of the Erineos
477 and Meganitis delta (Fig. 1). These sources are one of the main source of MTD 10 in sliding event F.

478

479 The seismic facies of most large MTDs also implies that they are likely composed mainly of fine-
480 grained sediments, and seismic profiles across fan-delta area have shown that the pro-delta foresets are
481 locally made of a thick accumulation of stratified fine-grained sediments. These fan-delta sediments are
482 probably the main source of sediments for the largest MTDs (MTD 10, 14 and 19). However, some
483 smaller MTDs seem to be made of coarser-grained sediments according to the seismic character (e.g., in

- Aurélia Ferrari 7/2/2018 15:09
Deleted: However,
- Aurélia Ferrari 7/2/2018 15:09
Deleted: t
- Aurélia Ferrari 7/2/2018 15:09
Deleted: rather than gravels typical of fan-deltas. S
- Aurélia Ferrari 7/2/2018 15:10
Deleted: in the Erineos
- Aurélia Ferrari 7/2/2018 15:11
Deleted: up to 90 m thick for the Holocene unit. Preserved between large gullies, these sediments display a surface slope of ~6°
- Aurélia Ferrari 7/2/2018 15:11
Deleted: They

493 SEs A and B in the Canyon basin), suggesting failure also occurred in coarser-grained parts of the fan-
494 deltas [located at the junction between the topset and the foreset beds](#) (e.g., the 1963 slide in the Erineos
495 fan-delta).

496 497 *5.3 Significance of the sliding events*

498
499 The data suggest that large submarine landslides have been triggered during six short periods of time
500 over the last 130 ka. These sliding events include variable numbers of [clustered](#) MTDs, from one (SE F)
501 to 8 (SE A). During three sliding events (C, D, F), a particularly large MTD accumulated at the basin
502 floor, and it has been shown that these large MTDs resulted from several possibly synchronous slope
503 failures. Similar MTD distributions have been observed in lakes in the Alps and in the Chilean Andes
504 (Strasser et al., 2013; Moernaut et al., 2007). In these studies, the correlation of MTDs into a same
505 "sliding event" was supported by radiocarbon dating and a simultaneous triggering has been proposed.
506 Correlations between the mass wasting records of neighbour lakes and the historical seismicity revealed
507 that most of these "sliding events" had been triggered by large earthquakes (Strasser et al., 2006;
508 Moernaut et al., 2007). In the westernmost Gulf of Corinth, neither coring, nor dating is available to
509 confirm our correlations between MTDs. Moreover, the occurrence of frequent turbidity currents
510 (Heezen et al., 1966; Lykousis et al., 2007a) and small-scale submarine landslides perturbs the sediment
511 layering and induces discontinuities in the seismic reflections, which makes MTD correlations based on
512 the seismic stratigraphy less accurate there than in many lakes.

513
514 The case of sliding event A demonstrates that MTDs grouped within the same event did not necessarily
515 occur at the same moment. Indeed, direct observation has shown that one MTD of this event occurred in
516 1963 AD and another in 1995 AD. By contrast, the synchronicity of different submarine landslides has
517 been suggested for SE C, D and F from the complex shape of the large MTDs they include. Though not
518 a proof, this lends support to the hypothesis of a seismic trigger of these three sliding events.

519
520 Consequently, the sliding events defined in this study may represent two different situations. In a first
521 case, they correspond to a period of time of 0.3 to 1 ka during which several submarine landslides of
522 various origins occurred. The sliding event A is such a case, with the coastal landslide caused in the
523 Meganitis delta area by the 1995 Aigion earthquake and an aseismic coastal landslide in the Erineos
524 delta area in 1963. The second case refers to likely simultaneous submarine landslides originating from
525 different slopes and forming a wide MTD of complex shape in the basin floor. An example of this case,
526 which is proposed to be earthquake-triggered, is the sliding event F, with a single MTD of complex
527 shape. Sliding events C and D possibly belong to this category as well. There is insufficient data to
528 allow for the determination of the nature of the minor events B and E.

529
530 Two main questions arise from these observations.

- 531 - Is seismicity the only forcing of SEs C, D and F or could other triggers or pre-conditioning factors
- 532 such as sediment supply and sea level change have influenced the system?
- 533 - What are possible trigger mechanisms and/or pre-conditioning factors responsible for a cluster of slope
- 534 failures such as SE A?

535
536 Urlaub et al. (2013) make inferences about controls on triggers of submarine landsliding from the
537 statistical analysis of the ages of 68 very large slides ($> 1 \text{ km}^3$) around the world. From a subset of 41
538 slides that occurred during the best documented last 30 ky, they show that the distribution of number of
539 events per ky resembles a Poisson distribution, suggesting that large submarine mass wasting might be
540 essentially random or, at best, that the global-scale signal for a climatic control, through either sea level
541 or sedimentation rate changes, is incoherent (non-uniform response of continental slopes worldwide) or
542 too weak to be expressed clearly with such a small sample size. They also note that, though strong
543 earthquakes might represent a temporally random trigger at the global scale, most of the slides in their
544 data set are located in low-seismicity passive continental margins (Urlaub et al., 2013). Here, we first
545 investigate the possible role of earthquakes through a comparative analysis of the frequency of sliding
546 events and earthquakes in the Gulf of Corinth area. Then, other potential controls will be discussed by
547 comparing the age distribution of the largest sliding events with published data about changes in

548 sediment dynamics and marine conditions in the Corinth Rift area. Owing to the small number of events
549 and high age uncertainties, which rule out statistical considerations, we provide only a qualitative
550 analysis.

551 552 5.4. *The possible role of large earthquakes*

553
554 The last four sliding events occurred during the last 10-12 ka, at an average rate of one event every 2.5-3
555 ka. Only two sliding events have been detected between ca. 130 ka and 10-12 ka. This *a priori*
556 surprising low frequency during the last glacial period (110-12 ka) with respect to the Holocene might
557 actually be somewhat biased by the fact that the seismic reflections corresponding to that period are less
558 clear (lower amplitude and lower continuity) than the reflections from the Holocene interval.
559 Consequently, medium-sized landslides such as those detected in SEs A and B might have been missed
560 in the seismic unit between reflectors 2 and 1.

561
562 The average recurrence interval for large earthquakes (Mw 6-7) has been estimated in the central part of
563 the Gulf of Corinth at ~500 yr during the Holocene, and ~400 yr for the period 12-17 ka, based on the
564 record of "homogenites" in the deepest part of the Gulf (Campos et al., 2013). In the western Gulf of
565 Corinth, estimates from palaeoseismological trenches on individual faults suggest an average recurrence
566 interval ≤ 360 yr on the Aigion fault (Pantosti et al., 2004), and of 200-600 yr on the East Helike fault
567 (McNeill et al., 2005) for the past 0.5-1 ka. It is clear, therefore, that large sliding events in the
568 westernmost Gulf of Corinth were less frequent than Mw 6-7 earthquakes, during both the Holocene and
569 the last glacial period. Consequently, while (anomalously?) large earthquakes could have triggered SEs
570 C, D and F, as suggested above from the geometry of MTDs 10, 14 and 19, it is likely that other factors
571 contributed to the occurrence of such large sliding events. These factors are explored in the next section.
572

573 5.5 *Other potential triggers and pre-conditioning factors*

574
575 Other possible processes that might have "pre-conditioned" or triggered sliding events in the Gulf of
576 Corinth need to show a return period of at least 2.5 ka over the last 12 ka in order to fit the SE
577 frequency. The following processes are proposed:
578 1. Sediment loading on top of a weak layer (e.g., gas-filled muddy sediments, as suggested for the area
579 by Lykousis et al. (2009)) (pre-conditioning factor);
580 2. Pulses of increased onshore erosion inducing temporary increase of sedimentation offshore, in turn
581 leading to slope overloading (pre-conditioning factor);
582 3. Sea level changes, which would have favoured slope failures during either lowstand conditions
583 (Perissoratis et al., 2000) or sea level rises (Zitter et al., 2012) (pre-conditioning factor);
584 4. Changes in the circulation and/or intensity of bottom-currents progressively destabilizing submarine
585 slopes through an increase in sedimentation or erosion rate (pre-conditioning factor);
586 5. Middle-term tectonic pulses, which would have temporarily increased the level of regional seismicity
587 (Koukouvelas et al., 2005; Demoulin et al., 2015) (trigger);
588 6. Loading by exceptional storm waves (trigger);
589 7. Large supply of coarse-grained sediments at a river mouth during exceptional flooding events
590 inducing slope failures by sediment overloading, as attested for the 1963 coastal landslide on the Erineos
591 fan-delta by Galanopoulos et al. (1964) (trigger).

592
593 All these hypotheses are not directly testable. Moreover, it is likely that different pre-conditioning
594 factors and triggers have interacted in various ways over the last 130 ka. Nevertheless, the four proposed
595 pre-conditioning factors can be discussed by comparing the SE age distribution with independent data
596 available for the region. We focus on the four events that mobilized a large volume of sediment ($\geq 10^8$
597 m³, SEs A, C, D, and F) because they probably indicate slope failures in different parts of the
598 westernmost Gulf, thus pointing to a regional signal. Even though these events have not been directly
599 dated by coring, ages can be reasonably inferred from the seismic stratigraphy. The most recent sliding
600 event (SE A) comprises MTDs at or near the sea floor and consequently occurred in the last 0.3-1 ka (a
601 range accounting for the thin layer of hemipelagites possibly covering some MTDs). Sliding event C
602 likely dates from the Mid-Holocene (~6-7 ka) according to the Holocene age-depth curve in the central

Aurélia Ferrari 7/2/2018 15:32

Deleted: that outcrop

604 part of the Gulf of Corinth (Campos et al., 2013). The two MTDs defining SE D occurred just after the
605 lacustrine to marine transition at the end of the Last Glacial, around 10-12 ka. Finally, the sliding event
606 F dates from sometime in the last glacial period.

607
608 Among the listed pre-conditioning factors, onshore erosion dynamics in the Corinth Rift area is the best
609 temporally documented. Fuchs (2007) presents the evolution of sedimentation rates in colluvial deposits
610 in the Phlious Basin, 25 km south of Xylocastro, for the last 10 ka (Fig. 9). He identifies two main
611 phases of land degradation between 6.5 and 8.5 ka, and from ~4 ka onwards. While the age of SE A
612 corresponds to the end of the most recent period of land degradation, the much more uncertain age of SE
613 C could correspond to the end of the land degradation phase at 6.5-8.5 ka (Fig. 9). The sliding event D is
614 too old to be compared with the results of Fuchs (2007). In brief, a relation might exist between periods
615 of high sediment supply from the watersheds and the occurrence of sliding events during the last 10 ky
616 (hypotheses 1 and 2).

617
618 Less information is available about Late Pleistocene sediment dynamics in the area. Collier et al. (2000)
619 suggest that the denudation rate in the Alkyonides Basin during the last glacial period (12-70 ka) was
620 almost twice those of the Holocene and MIS 5 interglacials. Instead, six radiocarbon dates on long cores
621 in the center of the Gulf of Corinth show a moderate increase in sedimentation rate between the end of
622 the last glacial period (17- 12 ka) and the Holocene (Campos et al., 2013). Overall, these data suggest
623 that the Last Glacial probably experienced the largest sedimentation rates over the last 130 ka in the
624 Gulf of Corinth. While the occurrence of the major SE F during this period again lends support to
625 increased sedimentation as a pre-conditioning factor of landsliding, it may however be surprising that no
626 other large sliding event has been recorded under such circumstances during the ~60 ky-long Last
627 Glacial.

628
629 Beside changes in erosion rates in the watersheds, the offshore realm underwent large changes between
630 the last glacial period and today. From 70 to 12 ka, the Gulf of Corinth was a lake and the water level
631 was around -60 m, assuming a constant depth of the Rion Sill over this period (Perissoratis et al., 2000).
632 At 10-12 ka, the rising waters in the Ionian Sea flooded the "Lake Corinth" through the Rion Sill
633 (Moretti et al., 2003; VanWelden 2007). The sea level continued to increase from ca. -60 m to its
634 present elevation until 5.5-6 ka, and bottom currents appeared in the study area (Beckers et al., 2016).
635 The deposition of SE D occurred at 10-12 ka, when the water level started to increase in the Corinth
636 Gulf. Water level increase and bottom current initiation might have favoured the destabilization of
637 sediments deposited during the preceding glacial period. In the Sea of Marmara, observations by Zitter
638 et al. (2012) and Beck et al. (2007) show an increase in large mass wasting events at the end of the last
639 lacustrine period and at the beginning of the marine period that likewise can be explained by a change in
640 oceanographic conditions, confirming the possible control of these pre-conditioning factors on SE D.

641
642
643
644 **Figure 9.** Comparison between the erosion dynamics over the last 10 ka from colluvial and alluvial archives
645 in the Peloponnese (Fuchs, 2007), the rate of local water level changes, and the occurrence of large sliding
646 events in the westernmost Corinth Rift during the Holocene. Bars without error bars in the second panel
647 indicate minimum sedimentation rates.

648

Aurélia Ferrari 13/2/2018 11:00

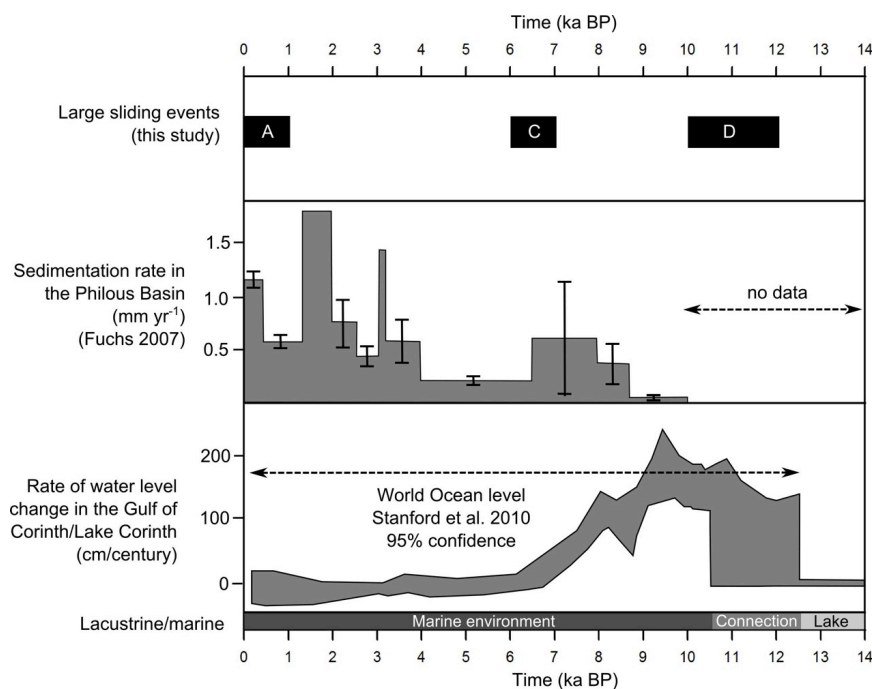
Deleted: 8

Aurélia Ferrari 13/2/2018 11:00

Deleted: 8

Aurélia Ferrari 13/2/2018 10:31

Deleted: 8



652
653
654

655 5.6 Conceptual model for the sliding events

656

657 Large sliding events (total volume $\geq 10^8 \text{ m}^3$) occurred in the westernmost Gulf of Corinth with fairly
658 long recurrence intervals, $\geq 2.5 \text{ ka}$. We suggest that their temporal distribution is primarily controlled by
659 changes in pre-conditioning factors, which were a prerequisite for any landslide trigger to be effective.

660

661 In other words, the clustering of slope failures during distinct sliding events would depend on the
662 appropriate state of pre-conditioning factors, which occur only during limited periods of time. Two
663 types of pre-conditioning factors may have played a significant role, on one hand increased denudation
664 rates, identified at 17-70 ka, 6.5-8.5 ka and 0-4 ka and, on the other hand, dramatic changes in
665 oceanographic conditions that occurred at 10-12 ka. More generally, the SE frequency would reflect the
666 time needed to reload submarine slopes beyond their stability threshold after each event. Once the pre-
667 conditioning factor evolution has made the slopes prone to sliding, each individual sliding event is
668 characterized by either simultaneous submarine landslides producing large coalesced MTDs and
669 pointing to a likely seismic trigger (SEs C, D and F) or separate smaller slides caused by various lower-
670 intensity triggers (earthquakes, exceptional onshore flood events, as exemplified by the 1995 and 1963
671 coastal landslides, respectively) over a few centuries (SE A).

671

672 Finally, we underline that the sliding processes have not been clearly identified in this study. Lykousis et
673 al. (2009) mention debris flows and avalanches for slope failures on steep fan-delta slopes ($2-6^\circ$) in the
674 western Gulf of Corinth, and rotational slumps on low angle ($0.5-2^\circ$) prodelta slopes. One sharp head
675 scarp identified in this study also shows that at least one translational slide happened in hemipelagites
676 accumulated far from the main river outlets.

677

678 5.7 Implications for tsunami hazard in the Gulf of Corinth

679

680 Among the 32 MTDs identified in this study, MTD 19 stands out as a particularly large feature (a little
681 less than 1 km^3 in volume). This is 6 times the volume of the second largest MTD identified in this

682 study, and about two orders of magnitude larger than the range previously proposed for the size of
683 submarine landslides in the westernmost Gulf of Corinth (Lykousis et al., 2007). It is also 6 times larger
684 than the largest MTD reported in the rest of the Gulf of Corinth, which occurred in the area of the
685 Perachora Peninsula (Papatheodorou et al., 1993; Stefatos et al., 2006). MTD 19 likely resulted from the
686 coalescence of at least two probably synchronous major slides. If correct, these slides should have
687 triggered very large tsunami waves, probably larger than those reported by historical sources in the
688 westernmost Gulf of Corinth, which were triggered by small to medium-sized slope failures
689 (Papadopoulos 2003; Stefatos et al., 2006; Tinti et al., 2007).

691 **6 Conclusion**

692
693 We documented the existence of large mass wasting events during the Holocene and the Late
694 Pleistocene in the westernmost Gulf of Corinth. Mass wasting events consist in submarine or coastal
695 landslides that occurred during short periods of time. Six large mass wasting events are listed, their
696 associated deposits locally representing 30% of the sedimentation since 130 ka in the Delphic Plateau
697 Basin. In the case of large MTDs (up to almost 1 km³ for the largest), a simultaneous triggering of
698 separate slope failures is proposed, suggesting a seismic origin. However, it is suggested that the
699 temporal distribution of sliding events is primarily controlled by the evolution of pre-conditioning
700 factors. Two main pre-conditioning factors are identified, namely (1) the time needed to slope reloading
701 after an event, which varied in relation with temporally varying sedimentation rates, and (2) dramatic
702 changes in water depth and water circulation that occurred 10-12 ka ago during the last post-glacial
703 transgression. Finally, it is likely that these sliding events have triggered large tsunami waves in the
704 whole Gulf of Corinth, in some cases (much?) larger than those reported in historical sources.

705
706 Competing interests. The authors declare they have no conflict of interest.

707
708 Acknowledgement. This work has been funded within the ANR SISCOR project directed by Pascal
709 Bernard, at Institut de Physique du Globe (Paris) and by FNRS- Grant for Researchers (CC) ID
710 14633841. Arnaud Beckers's PhD grant was supported by the Belgian FRIA. Funding for Arnaud
711 Beckers' stays in the ISTERre Laboratory was provided by a grant from la Région Rhône-Alpes. The
712 authors warmly acknowledge R/V ALKYON's crew, Koen De Rycker (RCMG), and Pascale Bascou
713 (ISTERre) for technical support, and the whole SISCOR scientific team for fruitful discussions.

714 **References**

- 715
716 Beck, C., Mercier de Lépinay, B., Schneider, J.-L., Cremer, M., Cagatay, N., Wendenbaum, E.,
717 Boutareaud, S., Ménot, G., Schmidt, S., Weber, O., Eris, K., Armijo, R., Meyer, B., & Pondard, N.
718 (2007). Late Quaternary co-seismic sedimentation in the Sea of Marmara's deep basins. *Sedimentary*
719 *Geology*, 199 (1-2), 65-89.
- 720
721 Beckers, A., Hubert-Ferrari, A., Beck, C., Bodeux, S., Tripsanas, E., Sakellariou, D., & De Batist, M.
722 (2015). Active faulting at the western tip of the Gulf of Corinth, Greece, from high-resolution seismic
723 data. *Marine Geology*, 360, 55-69.
- 724
725 [Beckers, A., 2015, Late quaternary sedimentation in the western gulf of Corinth : interplay between](#)
726 [tectonic deformation, seismicity, and eustatic changes, PhD thesis, pp. 260.](#)
- 727
728 Beckers, A., Beck, C., Hubert-Ferrari, A., Tripsanas, E., Crouzet, C., Sakellariou, D., Papatheodorou, G.
729 & De Batist, M. (2016). Influence of bottom currents on the sedimentary processes at the western tip of
730 the Gulf of Corinth, Greece. *Marine Geology*, 378, 312-332.
- 731
732 Beckers, A., Beck, C., Hubert-Ferrari, A., Reyss, J. L., Mortier, C., Albin, P., Rovida, A., Deville, A.-
733 L., Tripsanas, E., Sakellariou, D., Crouzet, C. & Scotti, O. (2017). Sedimentary impacts of recent
734 moderate earthquakes from the shelves to the basin floor in the western Gulf of Corinth. *Marine*
735 *Geology*, 384, 81-102.

737
738 Briole, P., Rigo, A., Lyon-Caen, H., Ruegg, J., Papazissi, K., Mitsakaki, C., Balodimou A., Veis G.,
739 Hatzfeld F., and Deschamps A. (2000). Active deformation of the Corinth rift, Greece: Results from
740 repeated Global Positioning System surveys between 1990 and 1995. *Journal of geophysical research*,
741 105 (B11), 25605-25625.
742
743 Campos, C., Beck, C., Crouzet, C., Carrillo, E., Welden, A. V., & Tripsanas, E. (2013). Late Quaternary
744 paleoseismic sedimentary archive from deep central Gulf of Corinth : time distribution of inferred
745 earthquake-induced layer. *Annals of Geophysics*, 56 (6), 1-15.
746
747 Collier, R. E., Leeder, M. R., Trout, M., Ferentinos, G., Lyberis, E., & Papatheodorou, G. (2000). High
748 sediment yields and cool, wet winters: Test of last glacial paleoclimates in the northern Mediterranean.
749 *Geology*, 28, 999-1002.
750
751 Cotterill, C. (2006). A High-resolution Holocene Fault Activity History of the Aigion Shelf, Gulf of
752 Corinth, Greece. PhD thesis, PhD Thesis, University of Southampton.
753
754 De Martini, P., Pavlopoulos, K., Pantosti, D., & Palyvos, N. (2007). 3HAZ Corinth Deliverable 73:
755 Dating of paleo-tsunamis. Tech. rep., Istituto Nazionale di Geofisica e Vulcanologia, Roma.
756
757 Demoulin, A., Beckers, A. & Hubert-Ferrari, A. (2015). Patterns of Quaternary uplift of the Corinth rift
758 southern border (N Peloponnese, Greece) revealed by fluvial landscape morphometry. *Geomorphology*
759 246, 188–204. doi:10.1016/j.geomorph.2015.05.032.
760
761 Ferentinos, G., Papatheodorou, G., & Collins, M. (1988). Sediment Transport processes on an active
762 submarine fault escarpment: Gulf of Corinth, Greece. *Marine Geology*, 83 (1-4), 43-61.
763
764 Fuchs, M. (2007). An assessment of human versus climatic impacts on Holocene soil erosion in NE
765 Peloponnese, Greece. *Quaternary Research*, 67 (3), 349-356.
766
767 Galanopoulos, A., Delimbasis, N., & Comninakis, P. (1964). A tsunami generated by a slide without a
768 seismic shock. *Geological Chronicles of Greece*, 16, 93-110.
769
770 Hasiotis, T., Charalampakis, M., Stefatos, a., Papatheodorou, G. & Ferentinos, G. (2006). Fan delta de-
771 velopment and processes offshore a seasonal river in a seismically active region, NW Gulf of Corinth.
772 *Geo-Marine Letters*, 26, 199–211. doi:10.1007/s00367-006-0020-8.
773
774
775 Heezen, B. C., Ewing, M., & Johnson, G. L. (1966). The Gulf of Corinth floor. *Deep-Sea research*, 13,
776 381-411.
777
778 Kontopoulos, N., & Avramidis, P. (2003). A late Holocene record of environmental changes from the
779 Aliko lagoon, Egean, North Peloponnese, Greece. *Quaternary International*, 111 (1), 75-90.
780
781 Koukouvelas, I. K., Katsonopoulou, D., Soter, S., & Xypolias, P. (2005). Slip rates on the Helike Fault,
782 Gulf of Corinth, Greece: New evidence from geoarchaeology. *Terra Nova*, 17 (2), 158-164.
783
784 Kortekaas, S., Papadopoulos, G.A., Ganas, A., Cundy, A., & Diakantoni, A. (2011). Geological
785 identification of historical tsunamis in the Gulf of Corinth, Central Greece. *Natural Hazards and Earth*
786 *System Science*, 11 (7), 2029-2041.
787
788 Lorito, S., Tiberti, M. M., Basili, R., Piatanesi, A., & Valensise, G. (2008). Earthquake-generated
789 tsunamis in the Mediterranean Sea: Scenarios of potential threats to Southern Italy. *Journal of*
790 *Geophysical Research*, 113 (B1), B01301.
791

792 Lykousis, V., Sakellariou, D., Rousakis, G., Alexandri, S., Kaberi, H., Nomikou, P., Georgiou P. &
793 Balas, D. (2007). Sediment failure processes in active grabens: the western gulf of Corinth (greece). in
794 V. Lykousis, D. Sakellariou, & J. Locat (Éds.), *Submarine Mass Movements and their Consequences III*
795 (pp. 297-305). Springer.
796
797 Lykousis, V., Roussakis, G., & Sakellariou, D. (2009). Slope failures and stability analysis of shallow
798 water prodeltas in the active margins of Western Greece, northeastern Mediterranean Se. *International*
799 *Journal of Earth Sciences*, 98 (4), 807-822.
800
801 McNeill, L., Cotterill, C., Henstock, T., Bull, J., Stefatos, A., Collier, R., Papatheoderou, G., Ferentinos,
802 G., & Hick S.E. (2005). Active faulting within the offshore western Gulf of Corinth, Greece:
803 Implications for models of continental rift deformation. *Geology*, 33 (4), 241.
804
805 Moernaut, J., De Batist, M., Charlet, F., Heirman, K., Chapron, E., Pino, M., Brümmer, R. & Urrutia, R.
806 (2007). Giant earthquakes in South-Central Chile revealed by Holocene mass-wasting events in Lake
807 Puyehue. *Sedimentary Geology* 195, 239–256. doi:10.1016/j.sedgeo.2006.08.005.
808
809 Moernaut, J., De Batist, M., Heirman, K., Van Daele, M., Pino, M., Brümmer, R., & Urrutia, R. (2009).
810 Fluidization of buried mass-wasting deposits in lake sediments and its relevance for paleoseismology:
811 Results from a reflection seismic study of lakes Villarrica and Calafquen (South-Central Chile).
812 *Sedimentary Geology*, 213 (3-4), 121-135.
813
814 Moernaut, J., & De Batist, M. (2011). Frontal emplacement and mobility of sublacustrine landslides:
815 Results from morphometric and seismostratigraphic analysis. *Marine Geology* 285 (2011) 29–45,
816 doi:10.1016/j.margeo.2011.05.001
817
818 Moernaut, J., Van Daele, M., Strasser, M., & De Batist, M. (2015). A lacustrine perspective on turbidite
819 and landslide cycles : implications for subaquatic paleoseismology. *Turbidites: process and records*, in:
820 Oral communication at the ISC 2015, Geneva.
821
822 Moretti, I., Lykousis, V., Sakellariou, D., Reynaud, J.-Y., Benziane, B., & Prinzhofer, A. (2004).
823 Sedimentation and subsidence rate in the Gulf of Corinth: what we learn from the Marion Dufresne's
824 long-piston coring. *Comptes Rendus Geoscience*, 336 (4-5), 291-299.
825
826 [Nomikou, P., Alexandri, M., Lykousis, V., Sakellariou, D., & Ballas, D. \(2011, September\). Swath](#)
827 [bathymetry and morphological slope analysis of the Corinth Gulf. In Grützner C. Pérez-López R,](#)
828 [Fernandez Steeger T. Papanikolaou I. Reicherter K. Silva PG & Vött A.\(eds\) Earthquake Geology and](#)
829 [Archaeology: Science, Society and Critical Facilities. 2nd INQUA-IGCP-567 International Workshop](#)
830 [on Active Tectonics, Earthquake Geology, Archeology and Engineering, 19-24.](#)
831
832 Pantosti, D., De Martini, P. M., Koukouvelas, I., Stamatopoulos, L., Palyvos, N., Pucci, S., Lemielle, F.,
833 & Pavlides, S. (2004). Palaeoseismological investigations of the Aigion Fault (Gulf of Corinth, Greece).
834 *Comptes Rendus Geoscience* , 336 (4-5), 335-342.
835
836 Papadopoulos, G. A. (2003). Tsunami Hazard in the Eastern Mediterranean : Strong Earthquakes and
837 Tsunamis in the Corinth Gulf , Central Greece. *Natural Hazards*, 29, 437-464.
838
839 Papatheodorou, G., & Ferentinos, G. (1993). Sedimentation processes and basin-filling depositional
840 architecture in an active asymmetric graben: Strava graben, Gulf of Corinth, Greece. *Basin Research* 5,
841 235–253. doi:10.1111/j.1365-2117.1993.tb00069.x.
842
843 Papatheodorou, G., & Ferentinos, G. (1997). Submarine and coastal sediment failure triggered by the
844 1995, M = 6.1 R Aegion earthquake, Gulf of Corinth , Greece. *Marine Geology*, 137, 287-304.
845

846 Papathoma, M., & Dominey-Howes, D. (2003). Tsunami vulnerability assessment and its implications
847 for coastal hazard analysis and disaster management planning, Gulf of Corinth, Greece. *Natural Hazards*
848 and *Earth System Science*, 3 (6), 733-747.

849

850 Perissoratis, C., Piper, D. J., & Lykousis, V. (2000). Alternating marine and lacustrine sedimentation
851 during late Quaternary in the Gulf of Corinth rift basin, central Greece. *Marine geology*, 167, 391-411.

852

853 Salamon, A., Rockwell, T., Ward, S. N., Guidoboni, E., & Comastri, A. (2007). Tsunami Hazard
854 Evaluation of the Eastern Mediterranean: Historical Analysis and Selected Modeling. *Bulletin of the*
855 *Seismological Society of America*, 97 (3), 705-724.

856

857 Soloviev, S. L. (1990). Tsunamigenic zones in the Mediterranean Sea. *Natural Hazards*, 3 (2), 183-202.

858

859 Stefatos, A., Charalambakis, M., Papatheodorou, G., & Ferentinis, G. (2006). Tsunamigenic sources in
860 an active European half-graben (Gulf of Corinth, Central Greece). *Marine Geology*, 232 (1-2), 35-47.

861

862 Strasser, M., Anselmetti, F. S., Fah, D., Giardini, D., & Schnellmann, M. (2006). Magnitudes and source
863 areas of large prehistoric northern Alpine earthquakes revealed by slope failures in lakes. *Geology*, 34
864 (12), 1005.

865

866 Strasser, M., Monecke, K., Schnellmann, M., & Anselmetti, F.S. (2013). Lake sediments as natural
867 seismographs: A compiled record of Late Quaternary earthquakes in Central Switzerland and its
868 implication for Alpine deformation. *Sedimentology*, 60, 319-341. doi:10.1111/sed.12003.

869

870 Tinti, S., Zaniboni, F., Armigliato, A., Pagnoni, G., Gallazzi, S., Manucci, A., Brizuela Reyes B.,
871 Bressan L., & Tonini, R., (2007). Tsunamigenic landslides in the western Corinth Gulf: numerical
872 scenarios. In V. Lykousis, & D. Sakellariou (Éds.), *Submarine Mass Movements and their*
873 *Consequences* (pp. 405-414). Springer.

874

875 Tripsanas, E. K. & Piper, D.J.W. (2008). Glaciogenic Debris-Flow Deposits of Orphan Basin, Offshore
876 Eastern Canada: Sedimentological and Rheological Properties, Origin, and Relationship to Meltwater
877 Discharge. *Journal of Sedimentary Research*, 78, 724-744.

878

879 Urlaub, M., Talling, P.J., & Masson, D.G. (2013). Timing and frequency of large submarine landslides:
880 Implications for understanding triggers and future geohazard. *Quaternary Science Reviews*, 72, 63-82.
881 URL: Link, doi:10.1016/j.quascirev.2013.04.020.

882

883 Van Welden, A. (2007). Enregistrements sédimentaires imbriqués d'une activité sismique et de
884 changements paléo-environnementaux. Etude comparée de différents sites: Golfe de Corinthe (Grèce),
885 Lac de Shkodra (Albanie/Montenegro), Golfe de Cariaco (Vénézuéla). PhD thesis, University of
886 Savoie

887

888 Woessner, J., Giardini, D., & Danciu, L. (2013). SHARE project, D5. "Final seismic hazard assessment
889 including aggregation. Tech. rep., Swiss Seismological Service.

890

891 Zitter, T.A.C., Grall, C., Henry, P., Ozeren, M.S., Cagatay, M.N., Sengor, A.M.C., Gasperini, L., de
892 Lépinay, B.M., & Géli, L. (2012). Distribution, morphology and triggers of submarine mass wasting in
893 the Sea of Marmara. *Marine Geology* 329-331, 58-74. doi:10.1016/j.margeo.2012.09.002.